Environmental Sciences Europe

RESEARCH

Open Access

Vertical distribution characteristics and potential sources of atmospheric pollutants in the North China Plain basing on the MAX-DOAS measurement

Guohua Liu[1] and Yu Wang[1,2*]

Abstract

The mechanism for the generation of atmospheric pollution sources can be further investigated through the examination of atmospheric evolution and diffusion characteristics. The authors of this study conducted a 3-month MAX-DOAS (multi-axis differential optical absorption spectroscopy) vertical observation in Shijiazhuang City, North China Plain, in the summer of 2020 in response to the long-standing air pollution issues in the region. The vertical distribution profiles of aerosol, NO_2, HCHO, and CHOCHO were generated, and the inversion findings showed good agreement with the TROPOMI (tropospheric monitoring instrument) satellite remote sensing validation, demonstrating the validity and accuracy of the observations. The near-surface boundary layer is home to the majority of the NO_2, HCHO, and CHOCHO species. The species' daytime evolution trends varied, with the highest NO_2 peaks occurring in the morning and evening commute, the highest HCHO peaks occurring in the morning at 10:00 a.m., and CHOCHO's concentration during the day declined. Two minor aerosol pollution processes took place in Shijiazhuang City during the summer observation period. The elevated concentrations of NO_2, CO, and the PM2.5/PM10 ratio during the pollution processes suggest that anthropogenic emissions, particularly biomass burning, were responsible for the large number of fine particles generated during the pollution events. Based on the examination of pollutant concentration profiles and meteorological data, it was determined that local emissions and north wind transport were the primary causes of Shijiazhuang's high NO_2 values. Meanwhile, the southern region of Shijiazhuang was primarily responsible for the majority of the potential sources of atmospheric HCHO, and local emissions were also a major factor affecting the high CHOCHO values. Shijiazhuang's local near-surface volatile organic compounds (VOCs) are mostly caused by human emissions, although biomass burning and its regional transportation have a greater influence on the middle and upper boundary layers. This study systematically sorted the evolution characteristics and potential sources of pollutants in Shijiazhuang City during the summer based on the joint observations of various pollutants, including NO_2, HCHO, and CHOCHO. These results can be used to support the development of appropriate policies for the prevention and control of pollutants in the Shijiazhuang local area of the North China Plain.

Keywords MAX-DOAS, Air pollutants, Pollution processes, Vertical profiles, Possible sources

*Correspondence:
Yu Wang
yuwang@ahu.edu.cn
[1] Institutes of Physical Science and Information Technology, Anhui University, Hefei 230601, China
[2] Information Materials and Intelligent Sensing Laboratory of Anhui Province, Anhui University, Hefei 230601, Anhui, China

Springer Open

© The Author(s) 2024. **Open Access** This article is licensed under a Creative Commons Attribution 4.0 International License, which permits use, sharing, adaptation, distribution and reproduction in any medium or format, as long as you give appropriate credit to the original author(s) and the source, provide a link to the Creative Commons licence, and indicate if changes were made. The images or other third party material in this article are included in the article's Creative Commons licence, unless indicated otherwise in a credit line to the material. If material is not included in the article's Creative Commons licence and your intended use is not permitted by statutory regulation or exceeds the permitted use, you will need to obtain permission directly from the copyright holder. To view a copy of this licence, visit http://creativecommons.org/licenses/by/4.0/.

Introduction

People who are exposed to polluted air for an extended period of time face serious risk to their health from the environment [1–3]. This risk includes respiratory and related cardiovascular diseases. Elevated levels of pollutants have the potential to damage urban structures, impair visibility in the atmosphere, and even lower agricultural productivity [4]. Over the last few decades, China's major urban agglomerations have seen a significant increase in primary pollutant emissions due to rapid urban development and rising motor vehicle ownership [5]. The North China Plain and the Beijing–Tianjin–Hebei (BJH) region have seen particularly high levels of fine particulate matter (PM2.5) and Ozone (O_3) pollution events [5–7]. Situated in the northern part of the North China Plain, the Beijing–Tianjin–Hebei region is a populous political and economic hub of China [8]. This area has always been the core region for research on environmental pollution [9, 10].

High concentrations of PM2.5, or fine particles suspended in the atmosphere with a diameter of less than 2.5 μm, are the primary cause of haze [11, 12]. Along with being the main source of direct emissions, PM2.5 and O_3 are significant atmospheric secondary pollutants [13–15]. Because of the intricacy of the secondary reaction production, these are mainly generated by a variety of air pollutants (such as sulfur dioxide, nitrogen oxides (NOX), volatile organic compounds (VOCs), and so on). [16]. The evidence of air haze, O_3 pollution, secondary pollution generation, and regional pollution characteristics has been mounting in recent years [17–19]. The pollution levels of PM2.5 and O_3 resulting from gaseous precursors in the secondary generation of a progressively higher percentage of the regional transmission flux have experienced a notable increase [20]. Research indicates that nitrate, sulfate, and other secondary aerosol concentrations in the Beijing–Tianjin–Hebei region will experience explosive growth during PM2.5 pollution events. Their contribution to PM2.5 will rise from 37.3% on weekdays to 56.9% during the pollution period, significantly raising the concentration of PM2.5 in the atmosphere [21, 22]. Furthermore, one of the main causes of pollution outbreaks is the horizontal and vertical transfer of pollutants [23]. Over the past 2 years, a number of studies have shown that the horizontal and vertical transfer of precursors and ozone may be the primary cause of the North China Plain's recurring summer pollution disasters [24]. Therefore, for the study of pollution causes and mechanisms, it is crucial to comprehend the spatial and temporal evolution characteristics of air pollutants and their precursors. In addition to the dearth of observational studies on the vertical distribution characteristics of these pollutants, prior research on air pollution has primarily concentrated on the evolutionary mechanisms of near-surface PM2.5 or O_3, with fewer reports on the observation of their common precursors.

An emerging ground-based optical remote sensing technique called ground-based multi-axis differential absorption spectroscopy (MAX-DOAS) allows one to simultaneously observe the concentration distribution of several air pollutants, including sulfur dioxide(SO_2), nitrogen dioxide (NO_2), formaldehyde (HCHO), nitrous acid (HONO), glyoxal (CHOCHO), and others [13, 25–28]. The sun's scattered light is gathered by the MAX-DOAS instrument from various elevation angles, resulting in a series of observations [29]. MAX-DOAS is an inexpensive device that can be used for long-term field observations and supports unattended field observations [30]. The gathered spectra can be quantitatively analyzed using the Lambert–Beer law to ascertain the integral concentrations of various pollutant components along the optical path. When paired with the best estimation technique, it is possible to invert several pollutants' vertical profiles at once.

MAX-DOAS has been widely used in the study of atmospheric pollution and the calibration of satellite observation, because it can simultaneously obtain the vertical profiles of pollutants and the total amount of tropospheric columns [31–34]. The characteristics of the vertical distributions of HCHO and NO_2 in the Huaihe River Basin were simultaneously obtained by Ren et al. [35], through an outfield observation conducted in September 2020 in Hefei, a key city in the Huaihe River Basin, based on MAX-DOAS observations. Subsequently, the authors examined the contribution law of the precursors' evolution to the production of ozone. An investigation of the effects of open burning of straw on the quality of the air near the Yangtze River was conducted by Tian et al. in June 2021 through observation experiments in three major cities in the Yangtze River Delta: Hefei, Nanjing, and Shanghai [36]. Between December 2018 and January 2019, Li et al. conducted aerosol observations in Sanmenxia. They looked into the vertical distribution of aerosols, source contribution, and the characterization of the different types of aerosols as well as the impact of PM2.5's chemical composition on aerosol extinction (AE) [33].

In Shijiazhuang, in the Beijing–Tianjin–Hebei region, we conducted ground-based MAX-DOAS observations for this study. In the summer of 2020, we concurrently acquired the total tropospheric columns (TTCs) and vertical column densities (VCDs) of aerosol extinction, NO_2, HCHO, and CHOCHO. Among them, the HCHO and NO_2 tropospheric column totals VCDs were validated with satellite observations; the results show good agreement, suggesting the accuracy and dependability of

the MAX-DOAS observations. In addition to analyzing the development and emission properties of these contaminants at different elevations, we also investigated the potential origins of NO2, HCHO, and CHOCHO in the Shijiazhuang region by integrating our results with data on the regional wind patterns.

Materials and methods

Introduction to observation experiments

To investigate the features of the vertical distribution of pollutants in the North China Plain during the summer, as well as the temporal evolution pattern and potential source areas, field observations were conducted in Shijiazhuang City, Hebei Province. Included in the observation period was MAX-DOAS, and it spanned the whole summer of 2020, from June 1 to August 31, 2020. The MAX-DOAS instrument was used for the outfield observation. It is situated approximately 15 m above the ground on the roof of the Hebei Artificial Weather Office (114.62° E, 37.91° N). The Hebei Provincial Weather Modification Office is situated in the southeast of Shijiazhuang, which is a city in Hebei Province. Shijiazhuang is situated in the southwest transmission corridor of Beijing. The site's southern portion is a sizable rural area, while the site's northern portion is a typical urban area. The location of Shijiazhuang in China is

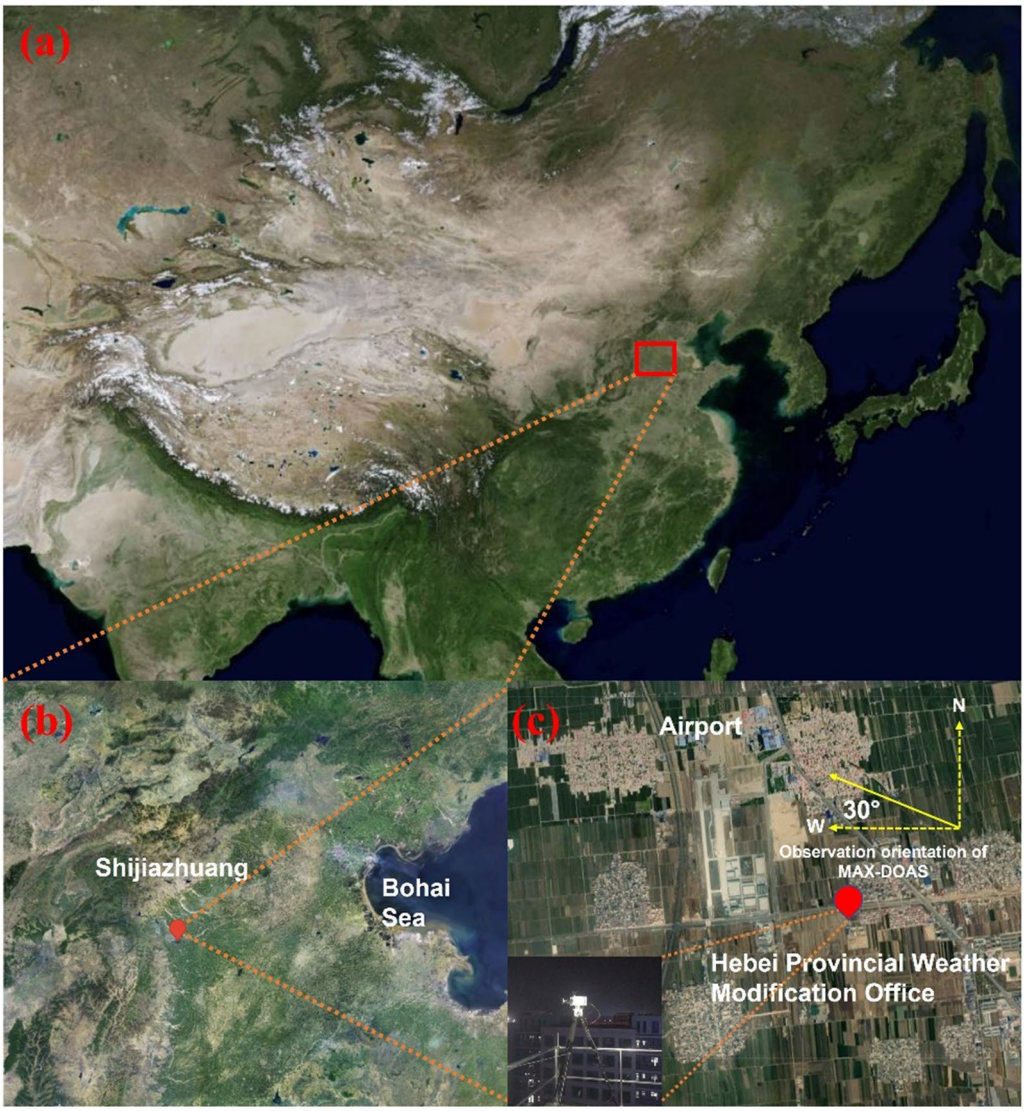

Fig. 1 Relative geographic location of observation sites [subfigure **a** shows the location of Shijiazhuang City in China, subfigure **b** shows the location of the sites relative to the North China Plain, and subfigure **c** shows the location of Shijiazhuang City, where the Hebei Provincial Weather Modification Office is located]

shown in Fig. 1a. The location of Shijiazhuang in China's North China Plain is shown in Fig. 1b, along with a satellite image map of the area in Fig. 1c. The scattered light from the sun in this direction is continuously collected at all elevation angles, with the instrument observation direction being 10° north by west.

Introduction to MAX-DOAS observation and data processing

The two main components of the MAX-DOAS instrument used in the observation experiments are the telescope outboard and the spectrometer inboard. The telescope outboard is equipped with two step motors to control the azimuth and elevation angles of the telescope, with an accuracy of less than 0.1° for the elevation motors. The telescope has a convex lens to converge the scattered light from the sun, and its field of view is less than 0.3°. The converged sunlight is directed by an optical fiber to the spectrometer inside the instrument, which is made up of two spectrometers (model AvaSpec-ULS2048L-USB2). The spectrometers cover the bands of 296–408 nm and 420–565 nm, respectively, and they have a spectral resolution of 0.60 nm. A 2048-pixel charge-coupled device (CCD) within the spectrometer transforms the optical signals into electrical signals. A bolometer regulates the spectrometer's temperature, and it maintains a steady 20 °C inside during the observation period, which can significantly lower the spectrometer's thermal noise. Using optical fibers, the sun-scattered light collected by the hyperspectral remote sensing instrument's outboard unit is fed into the spectrometer, where the sun-scattered spectra are left unsupervised for storage.

During the outfield observation, the azimuth of MAX-DOAS is set to 350°. The instrument automatically collects the scattered light from the sun during the day and the dark current and bias spectra during the night, and the entire process can be automatically controlled by a script on the industrial computer in unattended mode. The full measurement sequence of MAX-DOAS consists of 11 elevation angles of 1°, 2°, 3°, 4°, 5°, 6°, 8°, 10°, 15°, 30°, and 90°. The entire process can be automated by a script on the industrial computer in unattended mode.

MAX-DOAS spectral analysis

First, the solar spectra acquired by MAX-DOAS must be spectrally analyzed using the Lamb–Beer law. BIRA-IASB developed QDOAS software, which processes the data. The differential slant column densities (DSCDs), or the difference between the slant column densities (SCDs) on the observation path at the observation elevation angle and zenith angle, was obtained following spectral analysis. The specific parameters for the spectral analysis of oxygen dimer (O_4), NO_2, HCHO, and CHOCHO in this investigation are displayed in Table 1, with reference to earlier comparable studies. Among them, the spectral analysis bands of HCHO and CHOCHO were 336.5–359 nm and 431–460 nm, respectively, the spectral analysis bands ofO_4 and NO_2 were 338–370 nm, and the spectral analysis bands of O_4 and oxygen (O_2)is a dimer of atmospheric oxygen O, which is frequently utilized in MAX-DOAS observations to invert aerosol extinction coefficient profiles.

Figure 2 illustrates typical cases of spectral analysis fittings for these four trace gases. The black line represents the sum of the trace gas signals and the spectral fitting noise, while the red line represents the fitting results for the corresponding trace gases. The findings demonstrate that the signal-to-noise ratios of all four gases are good, and the spectral analysis is rational

Table 1 DOAS retrievals settings used for NO_2, O_4, HCHO, and CHOCHO DOAS spectral analysis

parameter	Data source	Fitting internal (nm)			
		O_4	NO_2	HCHO	Glyoxal
Wavelength range		338–370	338–370	322.5–358	431–461
NO_2	298K,I0 correction (SCDs of 1017 molecules cm^{-2}) Vandaele et al. [37]	√	√	√	√
NO_2	220K,I0 correction (SCDs of 1017 molecules cm^{-2}), pre-orthogonalized; Vandaele et al. [37]	√	√	×	√
O_4	293K; Thalman and Volkamer [38]	√	√	√	√
HCHO	297K; Meller and Moortgat [39]	√	√	√	×
CHOCHO	296K; Volkamer et al. [40]	×	×	×	√
Ring	Ring spectra calculated with QDOAS according to Chance and Spurr [41]	√	√	√	√
Polynomial degree		Order 3	Order 3	Order 5	Order 5
Intensity offset		Constant	Constant	Constant	Constant
Wavelength calibration	Based on a high-resolution solar reference spectrum (SAO2010 solar spectra); Chance and Kurucz [41]				

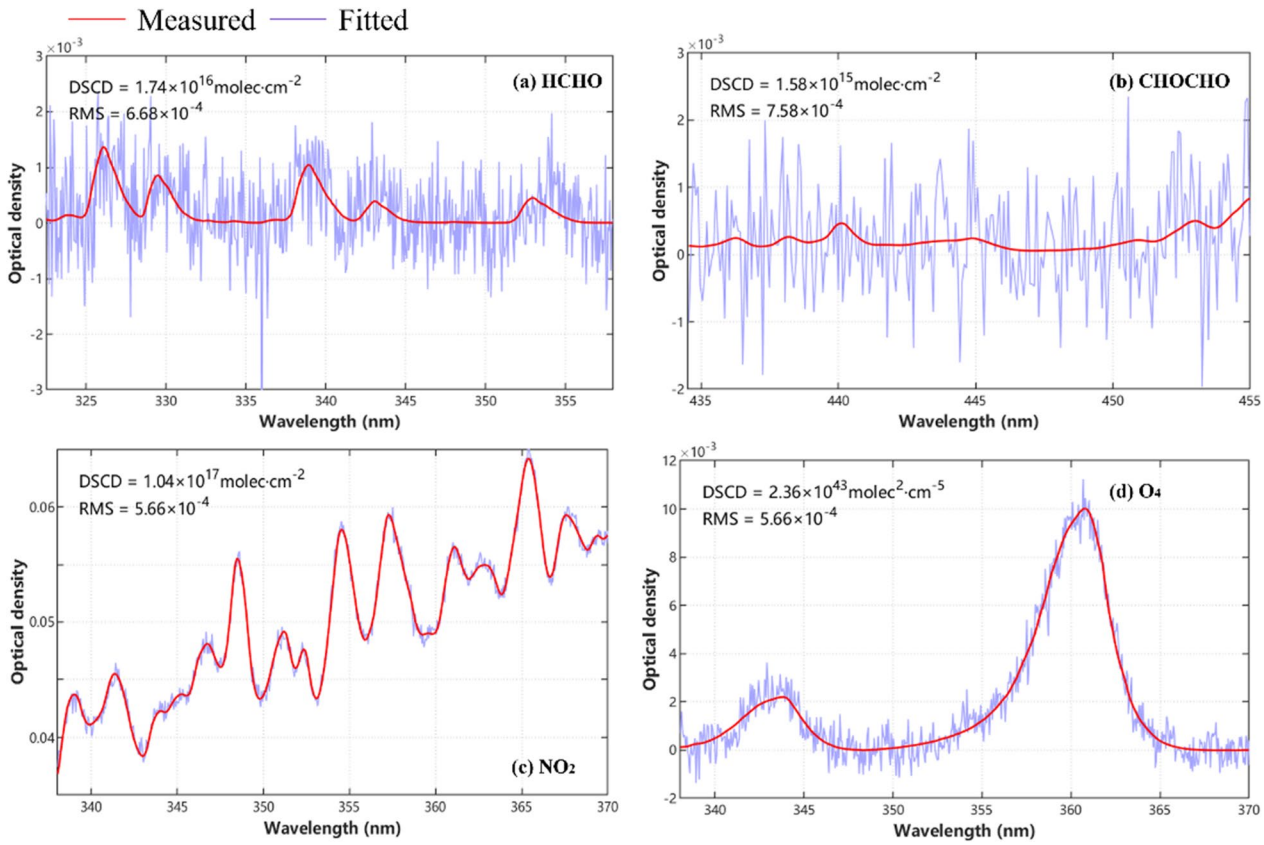

Fig. 2 Typical spectral analysis results for O_4, NO_2, HCHO, and CHOCHO (this spectrum is the x° solar scattering spectrum, taken at x time xx minutes)

and efficient enough to invert and produce the DSCDs signals in the spectra. To mitigate the impact of clouds on remote sensing accuracy, this study employed the color index method in conjunction with a first screening step that removed DSCDs with spectral analysis residual RMS greater than 2×10^{-3} before proceeding with further profile inversion (CI), in which the light intensity ratio at 330 nm to 390 nm was chosen as the indicator factor to determine the cloudy periods. To reduce analytical error, profile data were filtered out during the cloudy periods.

MAX-DOAS profile inversion

The DSCDs were inverted as a vertical contour of pollutant concentration as part of the MAX-DOAS further data analysis. This contour inversion was made possible by a profile inversion algorithm, which is based on the optimal estimation method (OEM) and uses SCIATRAN as the forward model for radiative transfer models [26, 42]. Using DSCDs observations and simulated values, the algorithm builds an iterative objective value function, which is displayed in Eq. 1. Nonlinear iterative inversion is then used to obtain the pollutant concentration contours [42]:

$$x^2 = \left(y - F(x,b)\right)^T S_\varepsilon^{-1}\left(y - F(x,b)\right) + (x - x_a)^T S_a^{-1}(x - x_a) \quad (1)$$

where $F(x,b)$ is the simulated value for the forward model of DSCDs, x is the vertical profile vector, b is the atmospheric parameters (such as temperature profile, surface albedo, a prior information, and atmospheric pressure) required for the forward model operation, y is the measured DSCDs, and x_a is the simulated value of the forward model DSCDs; S_ε and S_a are the covariance matrices of the measured value of the DSCDs, y, and the vertical profile vector, x_a, respectively. The process of inverting the aerosol and trace gas profiles involves two steps: first, the inversion yields the aerosol extinction coefficient profiles and the parameters of the aerosol optical thickness (AOD) based on the measured values of O_4 DSCDs at various observation elevation angles as inputs; second, the inversion of NO_2 is carried out using the aerosol extinction coefficient profiles and measured values of DSCDs for the trace gases as inputs and HCHO and

CHOCHO as inputs to invert the vertical profiles of trace gases, such as NO, HCHO, and CHOCHO.

The prior aerosol and trace gas profiles were set as profiles with a decreasing height e-index in the profile inversion. The near-surface 4 km altitude contours had a height resolution of 200 m from 2 to 4 km, and they were separated into 30 concentration-averaged layers within 2 km of the boundary layer. The near-surface concentrations of aerosols, NO_2, HCHO, and CHOCHO, were set at 0.2 km^{-1}, 5 ppbv, 2 ppbv, and 0.2 ppbv, respectively, and the scale height of a priori profile was 1 km. The aerosol optical parameters that were selected for the optimal estimation algorithm's parameterization were those that are typically found in urban areas: an asymmetry factor of 0.68, a single scattering albedo of 0.92, and a surface albedo of 0.05.

Presentation of other observational data

Meteorological data were used in this study to help analyze the possible sources of contribution of different pollutants in the presence of meteorological wind fields. The National Weather Service Science Data Center (http://data.cma.cn/) provided meteorological data for the following parameters: temperature, relative humidity, wind direction, and surface wind speed. The study utilized the meteorological data site number 536980, which is situated roughly 5 km away from the ground-based MAX-DOAS observation site.

Total HCHO, CHOCHO tropospheric columns observed by TROPOMI satellite

For a range of worldwide atmospheric pollutants (e.g., NO_2, HCHO, etc.), daily tropospheric pollutant level distribution results can be obtained from TROPOMI satellite observations [43–45]. The differential slant column concentration (DSCD) of a pollutant in the atmosphere is determined by spectral analysis using data from the TROPOMI satellite, which also computes the atmospheric mass factor (AMF) through forward radiative transfer simulation. The VCDs are obtained by dividing the DSCDs by the AMF. The observation angle of the satellite with respect to the sun and the data on atmospheric aerosols are input during the SCIATRAN forward simulation, from which the AMF is computed. Every day at 13:30 (Beijing time), the TROPOMI satellite transits, offering validation for ground-based MAX-DOAS observations with a horizontal resolution of 3.5 × 7 km.

Results

Observation results overview

Figure 3 shows the time series of aerosol optical thickness, PM2.5, PM10, and PM2.5/PM10, NO_2, carbon monoxide (CO), HCHO, CHOCHO, and the meteorological parameters of wind speed and direction, temperature, and humidity during the 3-month outfield observation period, which ran from June 1 to August 31, 2020. The average mass concentration of PM2.5 was 41.47 μg/m^3, PM10 was 69.21 μg/m^3, and the average aerosol optical thickness in Shijiazhuang, the observation site, was 1.06 in the summer. The trend of the aerosol optical thickness evolution process during the observation period was essentially the same as that of PM2.5 or PM10. Two major processes of aerosol pollution occurred throughout the summer observation period, from June 28 to July 5 and from August 4 to 13, respectively. The PM2.5/PM10 ratio increased in tandem with these two pollution processes, suggesting that fine particle generation was occurring concurrently with these processes, with PM2.5 accounting for the majority of aerosol extinction [26]. Higher CO concentrations were detected from the state control site during the second pollution process; these emissions could be linked to nearby fires or other primary combustion sources. With a near-surface mean concentration of 5.11 ppb, the observed atmospheric HCHO concentration was generally consistent throughout the summer observation period.

Validations of NO_2 and HCHO VCDs between MAX-DOAS and TROPOMI observation

To verify the accuracy of the NO_2 and HCHO results from the ground-based MAX-DOAS observations, here, the total tropospheric columns were obtained by integrating the NO_2 and HCHO contour concentrations from the ground-based MAX-DOAS observations in the summer of 2020 within the boundary layer along the height, and the correlation was verified with the VCDs at the Shijiazhuang site observed by TROPOMI satellite. Ground-based MAX-DOAS remote sensing inversion was used to obtain the NO_2 and HCHO vertical profiles, and the total NO_2 and HCHO columns in the boundary layer were obtained by integrating them along the height in the 0–3 km range of the profiles. Here, the MAX-DOAS contours were screened using the color index (CI) to make sure that clouds were not interfering with the data; previous research is cited for the screening procedure [46–48]. Meanwhile, only 1 h before and after the daily satellite transit moment (12:30 to 14:30 local time) of VCDs averaging was chosen for MAX-DOAS data to participate in the comparison validation to guarantee the consistency of the temporal representativeness of the ground-based and satellite observations. To obtain the VCDs, the satellite data were averaged over the four most adjacent observation grids centered on the latitude and longitude of the station.

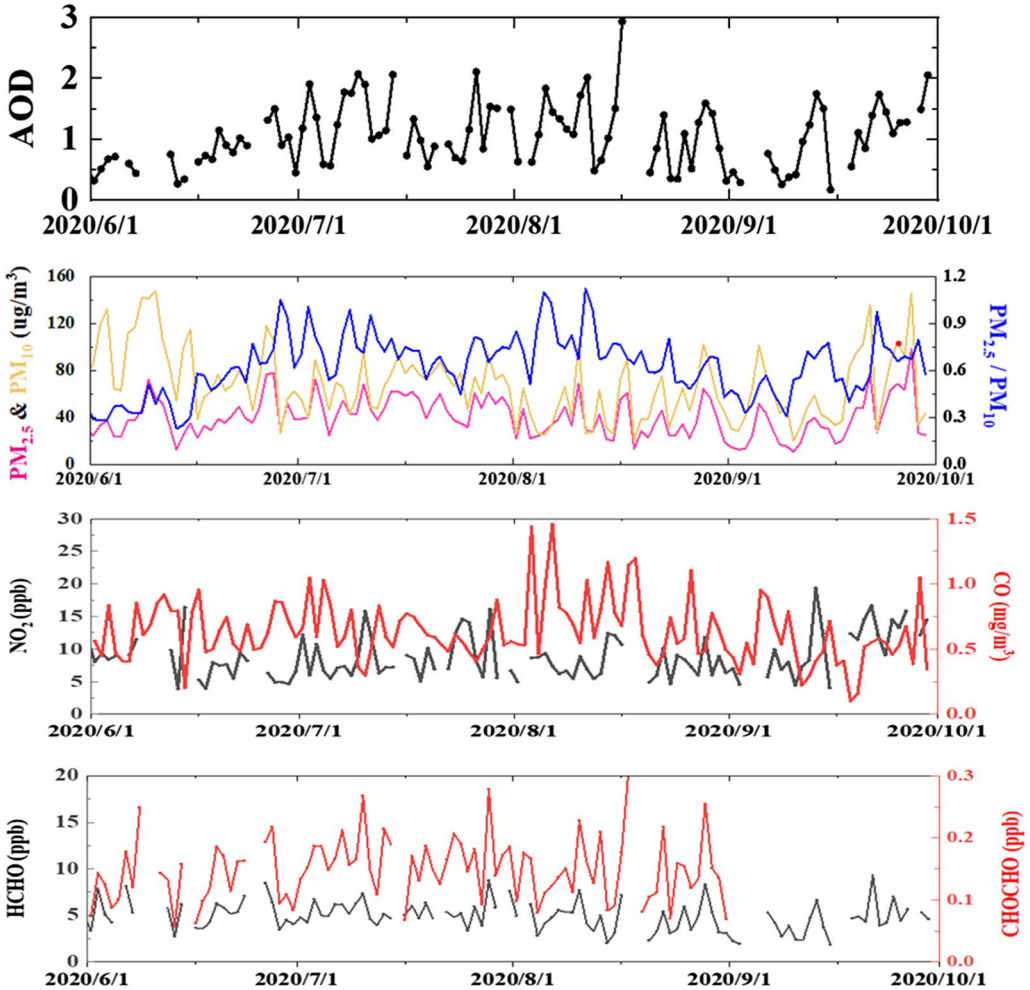

Fig. 3 Time series of pollutants and meteorological parameters from June to August 2020 (pollutants include: aerosols, PM2.5, PM10, NO_2, CO, HCHO, CHOCHO; meteorological parameters include: wind speed, temperature)

This ensured consistency between the spatial area of satellite observations and the ground-based MAX-DOAS observations.

Figure 4 displays the validation findings of the comparison between the MAX-DOAS and satellite remote sensing HCHO and NO_2 boundary layer column totals at the Shijiazhuang observation site during the summer of 2020. The tropospheric column total of HCHO in the two observations has a correlation validation coefficient R of 0.6, while the relevance of NO_2's VCDs reaches 0.667. These results show that, in the summer of 2020, there was good correlation between the satellite remote sensing tropospheric VCDs and ground-based MAX-DOAS observations, and there was consistency in the VCDs evolution trends of the monitored NO_2 and HCHO. The monitored NO_2 and HCHO VCD evolution trend consistency was good, and there was good correlation between the DOAS observation and satellite remote sensing tropospheric VCDs. These two observations can effectively track the evolution of pollutant concentrations. Furthermore, based on the correlation validation results' slope, it can be inferred that the total HCHO VCDs measured by TROPOMI were lower than those measured by MAX-DOAS. This discrepancy is primarily caused by the different sensitivity of MAX-DOAS observations and satellite remote sensing when it comes to measuring the vertical distribution of pollutants within the boundary layer. Because satellite observations primarily receive sunlight scattered upward from the atmosphere or the surface, ground-based MAX-DOAS observations primarily receive scattered light transmitted downward from the zenith.

The TROPOMI satellite primarily captures emissions from the sky to the ground, rendering it less sensitive to emissions in close proximity to the ground. Conversely,

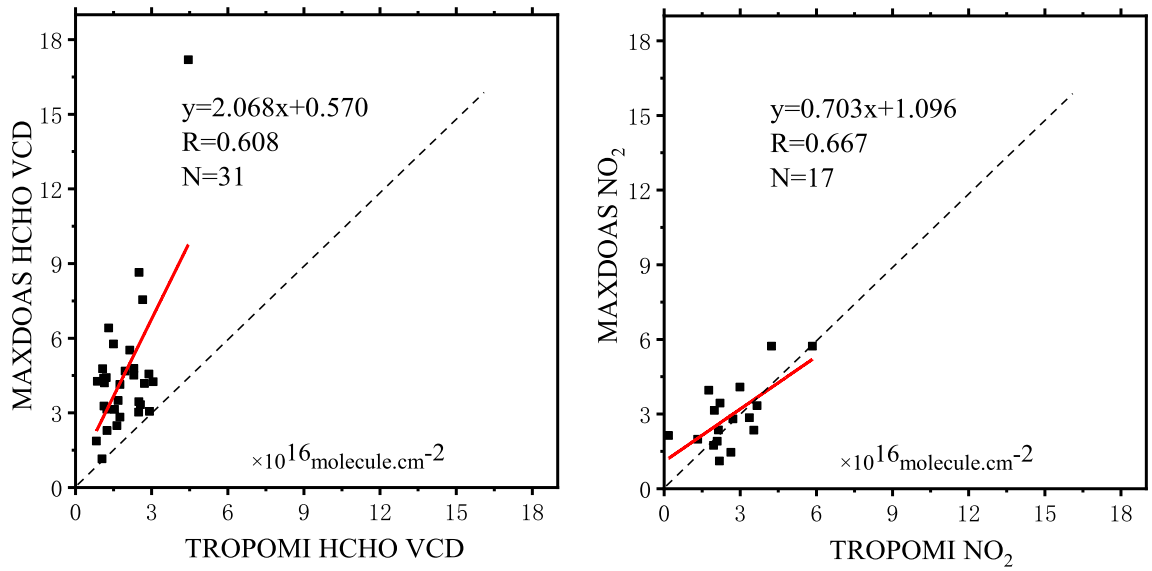

Fig. 4 Total tropospheric columns of HCHO and NO_2 observed by ground-based MAX-DOAS during the observation period, validated with TROPOMI satellite observations

the MAX-DOAS instrument observes emissions from the ground to the sky, making it more attuned to emissions near the ground level. This distinction has been highlighted in various scholarly articles [45, 49]. In addition, the study site for data collection is situated in a relatively remote area, encompassed by farmland and significant plant emissions. Consequently, there is a prevalence of primary sources of HCHO concentrated near the ground, while NO_2 primarily originates from vehicular and industrial emissions. The NO_2 levels observed in this study are predominantly influenced by regional high-altitude dispersion and emissions from elevated sources, resulting in a distribution at elevated altitudes. Consequently, the levels of HCHO observed by MAX-DOAS tend to be higher than those detected by TROPOMI, whereas the NO_2 levels observed by MAX-DOAS are lower than those recorded by TROPOMI. This pattern has also been noted in other research studies [50, 51].

As a result, MAX-DOAS is more sensitive to the distribution of pollutant concentrations in the boundary layer, especially near the surface. The majority of atmospheric HCHO is caused by primary emissions, with only a small contribution from the oxidation of secondary VOCs [52, 53]. This results in atmospheric HCHO concentrations in the boundary layer close to the ground. The VCDs of the satellite observations were smaller than those of the ground-based MAX-DOAS observations due to the vertical distribution characteristics of HCHO and NO_2, as well as the disparity in sensitivity between the two types of observations. The discrepancy between the VCDs of the TROPOMI satellite observations and the MAX-DOAS observations is also partially due to the differences between the two sets of observations. A contributing factor in the discrepancy between the TROPOMI and MAX-DOAS VCDs is the different effective area of the observations: the satellite observations are the average of the pollutant VCDs within the corresponding grid (3.5 km×7 km), while the VCDs from MAX-DOAS are more representative of the average pollutant conditions around the station.

Daily patterns of NO_2, HCHO, and CHOCHO in vertical direction

Clarifying the evolution patterns and possible sources of local pollutants in Shijiazhuang is made easier by analyzing the shifting patterns of pollutants like CHOCHO and HCHO. This study delved into the daily patterns of HCHO, NO_2, and CHOCHO in the boundary layer at different altitudes based on the vertical profiles of these pollutants that MAX-DOAS observed in Shijiazhuang, North China Plain, in summer 2020. In addition, the study examined the evolutionary correlations among these pollutants. To characterize the evolution of the bottom, middle, and top layers of the boundary layer, respectively, time series of the pollutant concentrations at 0–100 m, 300–400 m, and 700–800 m were chosen in the 0–3 km range contour of the boundary layer [54, 55]. The evolution of the pollutants at each height of the boundary layer was further investigated, and the daily changes in the NO_2, HCHO, and CHOCHO are displayed in Fig. 5.

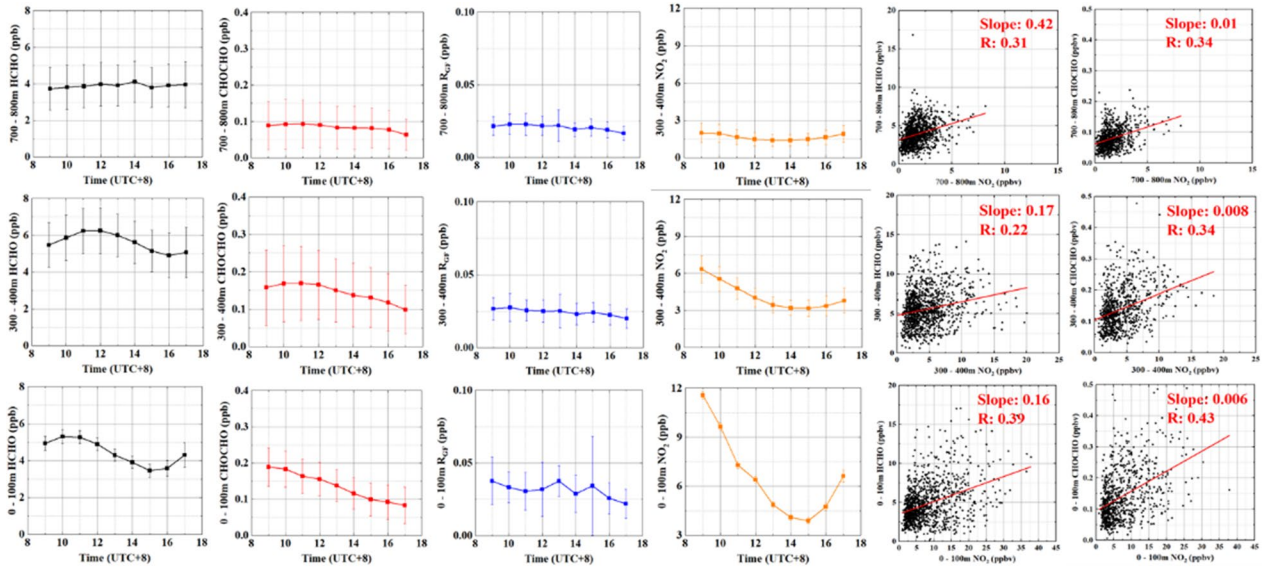

Fig. 5 Daily pattern of pollutants, such as HCHO, CHOCHO, NO2 in the bottom, middle, and top layers within the boundary layer

In Shijiazhuang City, the daily change process of every pollutant in the bottom layer of the boundary layer was the most noticeable, and every pollutant displayed a clear daily change process. The summer near-surface CHOCHO concentrations in Shijiazhuang City peaked in the morning, with an average of 0.189 ± 0.053 ppbv at 9:00 a.m. The concentration progressively dropped during the day to an average of 0.083 ± 0.050 ppbv at 5:00 p.m. The boundary layer's middle and lower layers held the majority of the vertical concentration of CHOCHO, while the near-surface had average daily concentrations of CHOCHO. The concentration of CHOCHO in the middle layer of the boundary layer and above decreased with altitude, and the average concentration in the layer of 700–800 m was 0.084 ± 0.059 ppbv. The average daily concentration of CHOCHO in the bottom and middle layers of the near-surface was 0.135 ± 0.047 ppbv and 0.144 ± 0.087 ppbv. The most noticeable daily variation was observed in the bottom layer of the near-surface for another pollutant, HCHO, which represents the activity of atmospheric VOC in its total amount. This pollutant reached its average concentration at 10 a.m. The process was most noticeable, occurring at other heights in the boundary layer and reaching a daily maximum mean concentration of 5.30 ± 0.38 ppbv at 10 a.m. and a minimum mean concentration of 3.45 ± 0.36 ppbv at 15 p.m. The daily average concentration of HCHO in the uppermost boundary layer was 3.90 ± 1.16 ppbv, and there was no discernible trend of change in this concentration. The primary source of HCHO and CHOCHO in the atmosphere is the oxidation of various VOCs. In the Shijiazhuang area, the high levels of HCHO and CHOCHO in the morning are primarily caused by OH oxidizing atmospheric VOCs during the previous night and releasing them into the atmosphere via aerosol in the morning [56]. The most noticeable daily variation in the NO_2 concentration in the atmosphere was also observed in the boundary layer's bottom 0–100 range; during the day, the NO_2 concentrations clearly displayed a "U" shape, with the highest concentration occurring at 9:00 a.m. The concentration progressively rose after 16:00 p.m., after which it gradually dropped in the morning and reached its lowest value of the day at around 15:00 p.m. As the altitude increased, the daily change rule of NO2 progressively decreased. The evolution of NO_2 with time and altitude is related to the source of atmospheric NO_2, which is primarily from motor vehicle emissions and fossil fuel combustion. Its peak time has a strong correlation with the daily morning and evening peaks. The daily pattern of variation decreased with altitude. Here, we simultaneously calculated the daily variation pattern of CHOCHO/HCHO (R_{GF}) based on the simultaneous observation of two atmospheric pollutants, CHOCHO and HCHO. R_{GF} has been widely used to characterize anthropogenic emissions in several previous studies, because although HCHO and CHOCHO are produced by the oxidation of different species of VOCs in the atmosphere, the CHOCHO concentration is more derived from anthropogenic source VOCs, while HCHO is more widely sourced, with both anthropogenic and natural sources [23]. Figure 5 illustrates a general trend of the gradual decrease in R_{GF} at all heights throughout the day, with the trend being more pronounced near the ground. This suggests that during the day, anthropogenic

VOC emissions, such as those from biomass burning, are more visible in Shijiazhuang. HCHO's boundary layer evolution differs greatly from CHOCHO's: in the near-surface layer, the concentration reaches a maximum value at 10 a.m., drops in the afternoon, and reaches a minimum value in the daytime at roughly 14 p.m. The reason for the high value in the morning is that the previous night's oxidation of the VOCs by OH radicals causes them to be released from the aerosol once more. In addition, significant photolytic oxidation products of VOCs, particularly isoprene, olefins, and aromatics are HCHO and CHOCHO in the near-surface layer and are linked to an increase in the concentrations of CHOCHO and HCHO after 15:00 p.m. HCHO exhibited an entirely different pattern of variation in the upper boundary layer: a "U"-shaped concentration evolution throughout the day, with the lowest concentration occurring at approximately 2.5 ppbv at 10:00 a.m. The middle boundary layer exhibited no discernible pattern of HCHO evolution. Primary emission and secondary generation are the two main sources of atmospheric HCHO, and high-altitude transport and secondary reaction generation properties largely determine how HCHO evolves in the middle and upper layers of the boundary layer.

The NO_2 concentration changes in a "U" shape on a daily basis. High values of the NO_2 concentration were primarily observed in the morning and evening peaks, close to the ground at 8:00 a.m. The maximum concentration was 10 ppbv. Because motor vehicle traffic volume and NO_2 concentration are clearly correlated, the concentration of NO_2 during the day was higher in the morning and evening. NO_2 is primarily produced by motor vehicle emissions near the ground, and the morning and evening concentrations are higher. The NO_2 concentration in the boundary layer decreases with height, because the majority of NO_2 emission sources are located close to the ground, and the evolution of the concentration is more noticeable the closer to the ground.

Discussion

RGF estimation

The concentration states of VOCs are influenced by various factors, including atmospheric VOCs concentration levels and pollutants, such as nitrogen oxides (NOx). These factors also determine the concentration levels and yields of HCHO and CHOCHO in the atmosphere. As a result, it is common practice to deduce the possible sources of atmospheric VOCs using the concentration ratio of CHOCHO to HCHO (R_{GF}) [26, 57, 58]. Prior research employing the R_{GF} factor has primarily examined the near-surface to ascertain the concentration ranges and plausible origins of HCHO and CHOCHO across various areas during varying seasons. This section examines the concentration levels and possible sources of VOCs at various elevations in the Shijiazhuang area of the North China Plain in the summer of 2020, based on the HCHO and CHOCHO concentration profiles.

Layer by layer and day by day, the concentration ratio was computed as R_{GF} based on the summer HCHO and CHOCHO concentration profiles in Shijiazhuang. The daily average sequences of R_{GF} and the range of evolution at different heights of the boundary layer in August 2020 are shown in Fig. 6. The daily mean values of R_{GF} at the bottom, middle, and upper levels of the boundary layer were 0.0205 ± 0.0077, 0.0864 ± 0.0296, and 0.0746 ± 0.0263, respectively. In August 2020, Shijiazhuang City's total near-surface R_{GF} was less than 0.04, indicating a changing process over time, with high values primarily occurring on August 14th, 19th, and 26th. Compared to the remaining days, which are more stable, these 3 days have a larger evolution range of R_{GF}. R_{GF} within the boundary layer increased gradually with altitude in a vertical direction, and the range of day-to-day variation also increased significantly. This suggests that the sources of VOCs in the upper and middle parts of the boundary layer are more complex and diverse as the altitude increases.

The amount of solar radiation, atmospheric OH radical concentrations, and atmospheric VOCs composition all have a direct impact on R_{GF} variation. Previous research has demonstrated that, even though thresholds for various VOCs sources may differ among locations, local sources of VOCs can still be inferred from factors with high or low levels. Broadly speaking, anthropogenic emissions dominate atmospheric VOCs when R_{GF} is small (i.e., less than 0.03); biomass dominates atmospheric VOCs emissions when R_{GF} is between 0.04

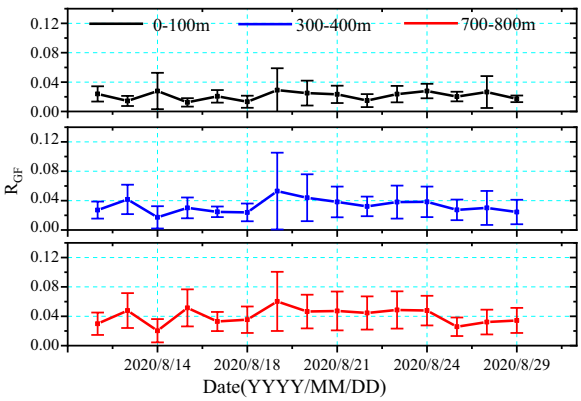

Fig. 6 Time series of R_{GF} at different heights of the boundary layer in the summer of 2020 in the Shijiazhuang area (at 0–100 m, 300–400 m, and 700–800 m height layers, respectively)

and 0.06; biomass combustion dominates when R_{GF} is greater than 0.5; and higher R_{GF} values may be indicative of anthropogenic activities, such as burning fossil fuels. This also suggests that human activity is the primary source of Shijiazhuang's local near-surface VOCs. The composition and concentration of local VOCs in Shijiazhuang will be influenced by the combustion of biomass, or even fossil fuels, and their regional transport, particularly in the middle and upper layers of the local boundary layer.

Analysis of potential sources of pollutants in the Shijiazhuang area

In addition to emissions from nearby anthropogenic sources, meteorological transport may also play a role in the local pollution in Shijiazhuang. To analyze the possible regional sources of the high local pollution values, wind rose diagrams of pollutant concentration versus wind field are investigated here. These are based on the vertical observation of pollutant profiles by MAX-DOAS in Shijiazhuang in summer 2020 and the wind speed and direction data of the local meteorological field in the same period. The link between summertime NO_2, HCHO, and CHOCHO concentrations and the direction and speed of the meteorological field at various elevations (0 m, 300 m, and 700 m) in the Shijiazhuang boundary layer is depicted in Fig. 7. High NO_2 concentrations in Shijiazhuang were frequently observed during the dominant northerly winds, as can be seen from the relationship between the concentrations and wind speed and direction. This suggests that the two main sources of local NO pollution in Shijiazhuang are the local NO emissions and regional transport from the north. In Shijiazhuang, regional transportation from the north and NO_2 emissions are the two main causes of local pollution. In Shijiazhuang, the two main sources of NO_2 close to the ground are local motor vehicle emissions and the combustion of fossil fuels. The vertical dependence of high NO_2 values on wind direction and speed gradually diminishes, suggesting that the regional NO_2 transport in Shijiazhuang has no discernible effect on the local boundary layer altitude. This study's observation station is southeast of Shijiazhuang City. The urban area north of the station is where the surrounding range's NO_2 values are highest, and any NO_2 that is released at one point will be dispersed throughout the surrounding area due to the

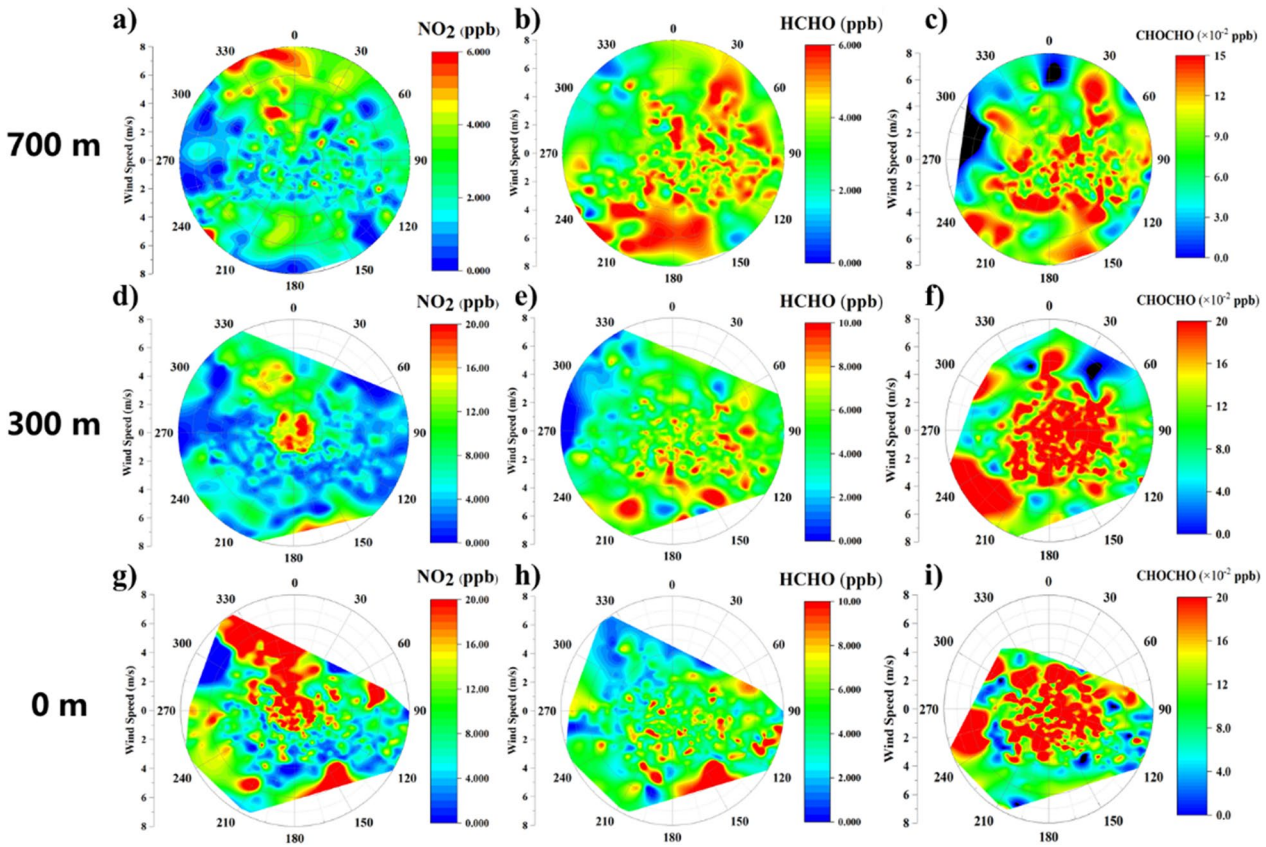

Fig. 7 Wind rose plot of NO_2, HCHO, and CHOCHO concentrations at different vertical heights in Shijiazhuang City in summer 2020 and their dependence on wind speed and wind direction

influence of the northerly wind and wind field. In the case of HCHO, the south wind is strongly correlated with the high values of HCHO at all boundary layer heights, and the southward transport contribution rises with height, suggesting that the south wind's regional transport has a greater impact on local HCHO in Shijiazhuang. HCHO is a significant intermediate product of atmospheric VOC oxidation. It can accurately characterize the total amount of VOCs in the atmosphere and has a strong correlation with the activity of the total VOCs. The wind-dependent plots of the HCHO concentration at each boundary layer height also show that regional transport between the city and the south is the primary source of VOCs in Shijiazhuang City. In the meantime, atmospheric HCHO is produced through reaction in the presence of precursors, since there are secondary sources of this gas. Consequently, compared to the near-surface bottom layer, the exogenous transport effect of high-altitude HCHO is more significant. Regarding the relationship between the high concentration of CHOCHO and the direction and speed of the wind, there does not seem to be any clear correlation. The primary emissions of anthropogenic sources account for the majority of the atmospheric CHOCHO, which is a useful indicator of anthropogenic volatile organic compounds. Consequently, it also suggests that Shijiazhuang's anthropogenic VOC sources are more uniform locally.

Conclusions

In the southeast of Shijiazhuang City, Hebei Province, China, we conducted MAX-DOAS outfield observations from June to August 2020. We obtained NO_2, HCHO, and CHOCHO profiles in the vertical range of 0–3 km. The intra-boundary layer VCDs were obtained by integrating the NO_2 and HCHO profiles that were recorded via MAX-DOAS. These VCDs were well-validated against the same-period observations of VCDs from the TROPOMI satellite, demonstrating the accuracy and dependability of the MAX-DOAS observations of tropospheric pollutants. The accuracy and reliability of MAX-DOAS's observation of tropospheric pollutants are demonstrated by the VCDs strong verification against the same timeframe of TROPOMI satellite observation. Two minor aerosol pollution events took place in Shijiazhuang throughout the summer observation period. The ratio of PM2.5/PM10 increased in both pollution processes, suggesting that a significant number of fine particles were produced in the pollution. Elevated NO_2 and CO concentrations, which are markers of human emissions, were present during the second pollution process, indicating that anthropogenic source emissions—particularly those from biomass burning—had a significant role in this pollution process. It was discovered that NO_2, HCHO, and CHOCHO were all primarily distributed near the surface of the boundary layer, based on the benefits of MAX-DOAS for the simultaneous vertical observation of multiple pollutants. However, the various species displayed distinct diurnal evolution trends, with high values in the morning and evening peaks of NO_2, a diurnal maximum at 10:00 a.m. and a minimum at 15:00 p.m. for HCHO, and decreasing diurnal concentrations for HCHO and CHOCHO. The primary reason for the variations in the evolution features of these three pollutants is their varying sources, and as the altitude increases, the trends of all three pollutants progressively decline. The potential sources of pollutants in Shijiazhuang during the summer were analyzed based on the pollutant concentration profiles and the meteorological wind speed and direction around the same station. The high value of NO_2 in Shijiazhuang was primarily caused by local emission and the influence of the north wind transmission, while the potential sources of atmospheric HCHO were primarily located in the southern region of Shijiazhuang, and the high value of CHOCHO was more due to the local emission. To assess the possible sources of VOCs at various elevations in Shijiazhuang during the summer, the R_{GF} factor was also applied here, based on the simultaneous observation of CHOCHO and HCHO by MAX-DOAS. It was discovered that human activity emissions were the primary source of the near-surface VOCs in Shijiazhuang. The local VOC components and concentrations in Shijiazhuang are influenced by the combustion of biomass or even fossil fuels and their regional transit, with regard to the middle and upper layers of the local boundary layer. The joint observation of multiple pollutants, including NO_2, HCHO, and CHOCHO by MAX-DOAS, summarizes the evolution characteristics and possible sources of summer pollutants in Shijiazhuang.

Acknowledgements
Thanks to the Remote Sensing Group of the University of Science and Technology of China for the support and help of ground remote sensing data. We thank the Belgian Institute for Space Aeronomy (BIRAIASB), Brussels, Belgium, for their freely accessible QDOAS software.

Author contributions
Conceptualization, G.L., and Y.W.; validation, Y.W.; writing—original draft, G.L.; writing—review and editing, Y.W.; software, G.L.; formal analysis, G.L.; resources, G.L., and Y.W.

Funding
This research was supported by grants from the Natural Science Foundation of Anhui Province (No. 2108085QF283), and the Natural Science Research Project of Colleges and Universities of Anhui Province (No. 2022AH050096).

Data availability
The data presented in this study are available on request from the corresponding author.

Declarations

Competing interests
The authors declare no competing interests.

Received: 24 January 2024 Accepted: 7 April 2024
Published online: 16 April 2024

References

1. Xing C, Liu C, Lin J, Tan W, Liu T (2023) VOCs hyperspectral imaging: a new insight into evaluate emissions and the corresponding health risk from industries. J Hazard Mater 461:132573. https://doi.org/10.1016/j.jhazmat.2023.132573
2. Gao M, Saide PE, Xin J, Wang Y, Liu Z, Wang Y, Wang Z, Pagowski M, Guttikunda SK, Carmichael GR (2017) Estimates of health impacts and radiative forcing in winter haze in eastern China through constraints of surface PM2.5 predictions. Environ Sci Technol 51:2178–2185
3. Lu X, Yao T, Fung JC, Lin C (2016) Estimation of health and economic costs of air pollution over the Pearl River Delta region in China. Sci Total Environ 566:134–143
4. Gong C, Liao H, Yue X, Ma Y, Lei Y (2021) Impacts of ozone-vegetation interactions on ozone pollution episodes in North China and the Yangtze River Delta. Geophys Res Lett 48:e2021GL093814
5. Wang Y, Gao W, Wang S, Song T, Gong Z, Ji D, Wang L, Liu Z, Tang G, Huo Y (2020) Contrasting trends of PM2.5 and surface ozone concentrations in China from 2013 to 2017. Natl Sci Rev. https://doi.org/10.1093/nsr/nwaa032
6. Zhai S, Jacob DJ, Wang X, Shen L, Li K, Zhang Y, Gui K, Zhao T, Liao H (2019) Fine particulate matter (PM2.5) trends in China, 2013–2018: separating contributions from anthropogenic emissions and meteorology. Atmos Chem Phys 19:11031
7. Song Y, Xing C, Liu C, Lin J, Wu H, Liu T, Lin H, Zhang C, Tan W, Ji X, Liu H, Li Q (2023) Evaluation of transport processes over North China Plain and Yangtze River Delta using MAX-DOAS observations. Atmos Chem Phys 23:1803–1824. https://doi.org/10.5194/acp-23-1803-2023
8. Vu TV, Shi Z, Cheng J, Zhang Q, He K, Wang S, Harrison RM (2019) Assessing the impact of clean air action on air quality trends in Beijing using a machine learning technique. Atmos Chem Phys 19:11303–11314
9. Wang Y, Konopka P, Liu Y, Chen H, Müller R, Plöger F, Riese M, Cai Z, Lü D (2012) Tropospheric ozone trend over Beijing from 2002–2010: ozonesonde measurements and modeling analysis. Atmos Chem Phys 12:8389–8399
10. Kang Y, Tang G, Li Q, Liu B, Cao J, Hu Q, Wang Y (2021) Evaluation and evolution of MAX-DOAS-observed vertical NO_2 profiles in urban Beijing. Adv Atmos Sci 38:1188–1196
11. Li B, Liu C, Hu Q, Sun M, Zhang C, Zhang S, Zhu Y, Liu T, Guo Y, Carmichael GR (2022) A deep learning approach to increase the value of satellite data for PM 2.5 monitoring in China. EGUsphere 2022:1–23
12. Wei J, Li Z, Lyapustin A, Sun L, Peng Y, Xue W, Su T, Cribb M (2021) Reconstructing 1-km-resolution high-quality PM2.5 data records from 2000 to 2018 in China: spatiotemporal variations and policy implications. Remote Sens Environ 252:112136
13. Ji X, Liu C, Wang Y, Hu Q, Lin H, Zhao F, Xing C, Tang G, Zhang J, Wagner T (2023) Ozone profiles without blind area retrieved from MAX-DOAS measurements and comprehensive validation with multi-platform observations. Remote Sens Environ 284:113339
14. Wang T, Xue L, Brimblecombe P, Lam YF, Li L, Zhang L (2017) Ozone pollution in China: a review of concentrations, meteorological influences, chemical precursors, and effects. Sci Total Environ 575:1582–1596
15. Xing C, Xu S, Song Y, Liu C, Liu Y, Lu K, Tan W, Zhang C, Hu Q, Wang S, Wu H, Lin H (2023) A new insight into the vertical differences in NO_2 heterogeneous reaction to produce HONO over inland and marginal seas. Atmos Chem Phys 23:5815–5834. https://doi.org/10.5194/acp-23-5815-2023
16. Ying Z, Tie X, Li G (2009) Sensitivity of ozone concentrations to diurnal variations of surface emissions in Mexico City: a WRF/Chem modeling study. Atmos Environ 43:851–859
17. Yu M, Tang G, Yang Y, Li Q, Wang Y, Miao S, Zhang Y, Wang Y (2020) The interaction between urbanization and aerosols during a typical winter haze event in Beijing. Atmos Chem Phys 20:9855–9870
18. Zhao Z, Liu R, Zhang Z (2020) Characteristics of winter haze pollution in the Fenwei plain and the possible influence of EU during 1984–2017. Earth Space Sci 7:e2020EA001134
19. Lin H, Xing C, Hong Q, Liu C, Ji X, Liu T, Lin J, Lu C, Tan W, Li Q, Liu H (2022) Diagnosis of ozone formation sensitivities in different height layers via MAX-DOAS observations in Guangzhou. J Geophys Res Atmos 127:e2022JD036803. https://doi.org/10.1029/2022JD036803
20. Liu C, Xing C, Hu Q, Li Q, Liu H, Hong Q, Tan W, Ji X, Lin H, Lu C, Lin J, Liu H, Wei S, Chen J, Yang K, Wang S, Liu T, Chen Y (2021) Ground-based hyperspectral stereoscopic remote sensing network: a promising strategy to learn coordinated control of O_3 and PM25 over China. Engineering. https://doi.org/10.1016/j.eng.2021.02.019
21. Huang X, Ding A, Wang Z, Ding K, Gao J, Chai F, Fu C (2020) Amplified transboundary transport of haze by aerosol–boundary layer interaction in China. Nat Geosci. https://doi.org/10.1038/s41561-020-0583-4
22. Dang R, Liao H (2019) Severe winter haze days in the Beijing–Tianjin–Hebei region from 1985 to 2017 and the roles of anthropogenic emissions and meteorology. Atmos Chem Phys 19:10801–10816
23. Ji X, Hu Q, Hu B, Wang S, Liu H, Xing C, Lin H, Lin J (2021) Vertical structure of air pollutant transport flux as determined by ground-based remote sensing observations in Fen-Wei Plain. China Remote Sens 13:3664
24. Chang X, Wang S, Zhao B, Cai S, Hao J (2018) Assessment of inter-city transport of particulate matter in the Beijing-Tianjin-Hebei region. Atmos Chem Phys 18:4843–4858
25. Ma J, Dörner S, Donner S, Jin J, Cheng S, Guo J, Zhang Z, Wang J, Liu P, Zhang G (2020) MAX-DOAS measurements of NO_2, SO_2, HCHO, and BrO at the Mt. Waliguan WMO GAW global baseline station in the Tibetan Plateau. Atmos Chem Phys 20:6973–6990
26. Xing C, Liu C, Hu Q, Fu Q, Lin H, Wang S, Su W, Wang W, Javed Z, Liu J (2020) Identifying the wintertime sources of volatile organic compounds (VOCs) from MAX-DOAS measured formaldehyde and glyoxal in Chongqing, southwest China. Sci Total Environ 715:136258
27. Xue J, Zhao T, Luo Y, Miao C, Su P, Liu F, Zhang G, Qin S, Song Y, Bu N (2022) Identification of ozone sensitivity for NO_2 and secondary HCHO based on MAX-DOAS measurements in northeast China. Environ Int 160:107048
28. Hong Q, Zhu L, Xing C, Hu Q, Lin H, Zhang C, Zhao C, Liu T, Su W, Liu C (2022) Inferring vertical variability and diurnal evolution of O_3 formation sensitivity based on the vertical distribution of summertime HCHO and NO_2 in Guangzhou, China. Sci Total Environ 827:154045
29. Chan KL, Wang Z, Ding A, Heue K-P, Shen Y, Wang J, Zhang F, Shi Y, Hao N, Wenig M (2019) MAX-DOAS measurements of tropospheric NO_2 and HCHO in Nanjing and a comparison to ozone monitoring instrument observations. Atmos Chem Phys 19:10051–10071
30. Lin H, Liu C, Xing C, Hu Q, Hong Q, Liu H, Li Q, Tan W, Ji X, Wang Z (2020) Validation of water vapor vertical distributions retrieved from MAX-DOAS over Beijing, China. Remote Sens 12:3193
31. Schreier SF, Bösch T, Richter A, Lange K, Revesz M, Weihs P, Vrekoussis M, Lotteraner C (2021) Evaluation of UV–visible MAX-DOAS aerosol profiling products by comparison with ceilometer, sun photometer, and in situ observations in Vienna, Austria. Atmos Meas Tech 14:5299–5318
32. Wang Y, Lampel J, Xie P, Beirle S, Li A, Wu D, Wagner T (2017) Ground-based MAX-DOAS observations of tropospheric aerosols, NO_2, SO_2 and HCHO in Wuxi, China, from 2011 to 2014. Atmos Chem Phys 17:2189–2215
33. Li X, Xie P, Li A, Xu J, Ren H, Ren B, Li Y, Li J (2021) Study of aerosol characteristics and sources using MAX-DOAS measurement during haze at an urban site in the Fenwei Plain. J Environ Sci 107:1–13
34. Liu C, Xing C, Hu Q, Wang S, Zhao S, Gao M (2022) Stereoscopic hyperspectral remote sensing of the atmospheric environment: innovation and prospects. Earth Sci Rev 226:103958. https://doi.org/10.1016/j.earscirev.2022.103958
35. Ren B, Xie P, Xu J, Li A, Qin M, Hu R, Zhang T, Fan G, Tian X, Zhu W, Hu Z, Huang Y, Ii X, Meng F, Zhang G, Tong J, Ren H, Zheng J, Zhang Z, Lv Y (2022) Vertical characteristics of NO_2 and HCHO, and the ozone formation regimes in Hefei, China. Sci Total Environ 823:153425
36. Tian X, Ren B, Xie P, Xu J, Li A, Hu F, Zheng J, Ren H, Hu Z, Pan Y, Huang X, Zhang Z, Lv Y, Tian W, Wang Z (2022) The vertical distribution and potential sources of aerosols in the Yangtze River Delta region of China during open straw burning. Sci Total Environ 849:157749

37. Vandaele AC, Hermans C, Simon PC, Carleer M, Colin R, Fally S, Merienne M-F, Jenouvrier A, Coquart B (1998) Measurements of the NO_2 absorption cross-section from 42,000 cm^{-1} to 10,000 cm^{-1} (238–1000 nm) at 220 K and 294 K. J Quant Spectrosc Radiat Transf 59:171–184
38. Thalman R, Volkamer R (2013) Temperature dependent absorption cross-sections of O_2–O_2 collision pairs between 340 and 630 nm and at atmospherically relevant pressure. Phys Chem Chem Phys 15:15371–15381
39. Meller R, Moortgat GK (2000) Temperature dependence of the absorption cross sections of formaldehyde between 223 and 323 K in the wavelength range 225–375 nm. J Geophys Res Atmos 105:7089–7101
40. Volkamer R, Spietz P, Burrows J, Platt U (2005) High-resolution absorption cross-section of glyoxal in the UV–vis and IR spectral ranges. J Photochem Photobiol A Chem 172:35–46
41. Chance K, Kurucz RL (2010) An improved high-resolution solar reference spectrum for earth's atmosphere measurements in the ultraviolet, visible, and near infrared. J Quant Spectrosc Radiat Transfer 111:1289–1295
42. Xing C, Liu C, Wang S, Chan KL, Gao Y, Huang X, Su W, Zhang C, Dong Y, Fan G, Zhang T, Chen Z, Hu Q, Su H, Xie Z, Liu J (2017) Observations of the vertical distributions of summertime atmospheric pollutants and the corresponding ozone production in Shanghai China. Atmos Chem Phys 17:14275–14289. https://doi.org/10.5194/acp-17-14275-2017
43. Lin J, Xing C, Liu C, Tan W, Wang W, Wu P, Lu C, Li Q, Liu T (2023) Hyperspectral imaging technique supports dynamic emission inventory of coal-fired power plants in China. Sci Bull 68:1248–1251. https://doi.org/10.1016/j.scib.2023.05.020
44. Zhao F, Liu C, Cai Z, Liu X, Bak J, Kim J, Hu Q, Xia C, Zhang C, Sun Y (2021) Ozone profile retrievals from TROPOMI: implication for the variation of tropospheric ozone during the outbreak of COVID-19 in China. Sci Total Environ 764:142886
45. Su W, Liu C, Chan KL, Hu Q, Liu H, Ji X, Zhu Y, Liu T, Zhang C, Chen Y (2020) An improved TROPOMI tropospheric HCHO retrieval over China. Atmos Meas Tech 13:6271–6292
46. Kreher K, Van Roozendael M, Hendrick F, Apituley A, Dimitropoulou E, Frieß U, Richter A, Wagner T, Lampel J, Abuhassan N et al (2020) Intercomparison of NO_2, O_4, O_3 and HCHO slant column measurements by MAX-DOAS and zenith-sky UV-Visible spectrometers during the CINDI-2 campaign. Atmos Meas Tech 13:2169–2208. https://doi.org/10.5194/amt-13-2169-2020
47. Beirle S, Wagner T et al (2016) Absolute calibration of the colour index and O-4 absorption derived from Multi AXis (MAX-)DOAS measurements and their application to a standardised cloud classification algorithm. Atmos Meas Tech 9(9):4803–4823
48. Ren B, Xie P, Xu J, Li A, Tian X, Hu Z, Huang Y, Li X, Zhang Q, Ren H et al (2021) Use of the PSCF method to analyze the variations of potential sources and transports of NO_2, SO_2, and HCHO observed by MAX-DOAS in Nanjing, China during 2019. Sci Total Environ 782:146865. https://doi.org/10.1016/j.scitotenv.2021.146865
49. Vigouroux C, Langerock B, Bauer Aquino CA, Blumenstock T, Cheng Z, De Mazière M, De Smedt I, Grutter M, Hannigan JW, Jones N, Kivi R, Loyola D, Lutsch E, Mahieu E, Makarova M, Metzger J-M, Morino I, Murata I, Nagahama T, Notholt J, Ortega I, Palm M, Pinardi G, Röhling A, Smale D, Stremme W, Strong K, Sussmann R, Té Y, van Roozendael M, Wang P, Winkler H (2020) TROPOMI–Sentinel-5 precursor formaldehyde validation using an extensive network of ground-based Fourier-transform infrared stations. Atmos Meas Tech 13:3751–3767. https://doi.org/10.5194/amt-13-3751-2020
50. Makar PA, Staebler RM, Akingunola A, Zhang J, McLinden C, Kharol SK, Pabla B, Cheung P, Zheng Q (2017) The effects of forest canopy shading and turbulence on boundary layer ozone. Nat Commun 8(1):15243
51. Qihou Hu, Ji X, Hong Q, Li J, Li Q, Jinping Ou, Liu H, Xing C, Tan W, Chen J, Chang B, Liu C (2024) Vertical evolution of ozone formation sensitivity based on synchronous vertical observations of ozone and proxies for its precursors: implications for ozone pollution prevention strategies. Environ Sci Technol 58(9):4291–4301
52. Geiger H, Kleffmann J, Wiesen P (2002) Smog chamber studies on the influence of diesel exhaust on photosmog formation. Atmos Environ 36(11):1737–1747. https://doi.org/10.1016/S1352-2310(02)00175-9
53. Li X, Brauers T, Hofzumahaus A, Lu K, Li Y, Shao M et al (2013) MAX-DOAS measurements of NO2, HCHO and CHOCHO at a rural site in southern China. Atmos Chem Phys 13(4):2133–2151. https://doi.org/10.5194/acp-13-2133-2013
54. Luo YH, Sun LG, Liu WQ et al (2012) MAX-DOAS measurements of NO_2 column densities and vertical distribution at Ny-Alesund, Arctic during summer. Spectrosc Spectr Anal 32(9):2336–2340. https://doi.org/10.3964/j.issn.1000-0593(2012)09-2336-05
55. Li MC, Yang YJ, Guo J et al (2014) Numerical modeling of local air pollutant dispersion characteristics in Tianjin Binhai New Area. Chin J Ecol 33(3):748–754
56. Volkamer R, San Martini F, Molina LT, Salcedo D, Jimenez JL, Molina MJ (2007) A missing sink for gas-phase glyoxal in Mexico City: formation of secondary organic aerosol. Geophys Res Lett 34:LI9807. https://doi.org/10.1029/2007GL030752
57. Vrekoussis M, Wittrock F, Richter A, Burrows JP (2010) GOME-2 observations of oxygenated VOCs: what can we learn from the ratio glyoxal to formaldehyde on a global scale? Atmos Chem Phys 10(21):10145–10160. https://doi.org/10.5194/acp-10-10145-2010
58. Ortega I, Koenig T, Sinreich R, Thomson D, Volkamer R (2015) The CU 2-D-MAX-DOAS instrument—part 1: retrieval of 3-D distributions of NO2 and azimuth-dependent OVOC ratios. Atmos Meas Tech. https://doi.org/10.5194/amt-8-2371-2015

Publisher's Note

Springer Nature remains neutral with regard to jurisdictional claims in published maps and institutional affiliations.